WIDE ANGLE FD AND FFD MIGRATION USING COMPLEX PADÉ APPROXIMATIONS

D. Amazonas, J. C. Costa, R. Pestana, and J. Schleicher

email: *daniela.amazonas@gmail.com*
keywords: *Depth migration, complex Padé approximation*

ABSTRACT

Seismic Migration by downward continuation using the one-way wave equation approximations has two shortcomings: imaging steep dip reflectors and handling evanescent waves. Complex Padé approximations allow a better treatment of evanescent modes, stabilizing finite-difference migration without requiring special treatment for the migration domain boundaries. Imaging steep dip reflectors can be improved using several terms in the Padé expansion. We discuss the implementation and evaluation of wide-angle complex Padé approximations for finite-difference and Fourier finite-difference migration methods. The dispersion relation and the impulsive response of the migration operator provide criteria to select the number of terms and coefficients in the Padé expansion. This assures stability for a prescribed maximum propagation direction. The implementations are validated on the Marmousi model dataset and SEG/EAGE salt model data.

INTRODUCTION

Wave equation migration algorithms have a better performance than ray-based migration when the velocity model has strong lateral velocity variations. Among several existing algorithms for wave-equation migration, finite-difference (FD) and Fourier finite-difference (FFD) migrations (Ristow and Rühl, 1994) can provide wide-angle approximations for the one-way continuation operators, thus improving the imaging of steep dip reflectors.

However, standard (real-valued) FD and FFD migrations cannot handle evanescent waves correctly (Millinazzo et al., 1997). As a consequence, FFD algorithms tend to become numerically unstable in the presence of high velocity variations (Biondi, 2002). To overcome this limitation, Biondi (2002) proposed an unconditionally stable extension for the FFD algorithm. Earlier, Millinazzo et al. (1997) proposed a different approach to treating these evanescent modes in ocean acoustic applications. They introduced an extension of the Padé approximation which they called complex Padé.

The complex Padé expansion was used previously in applied geophysics. Zhang et al. (2003) used the method in finite-difference migration. However, their implementation were not suited for wide angles. Later, Zhang et al. (2004) proposed a split-step migration based on complex Padé.

In this paper, we study the use of the complex Padé expansion for wide-angle FD and FFD pre-stack depth migration algorithms. The expansion is evaluated numerically, comparing its approximation to the exact one-way operator. Based on studying the impulse response of the migration operator, we propose a prescription to choose parameters for wide-angle complex FD and FFD algorithms. The algorithms are validated on synthetic datasets from the Marmousi and SEG/EAGE salt models.

METHODOLOGY

Complex Padé approximation

The one-way wave equation for downward continuation of the acoustic wavefield reads (Ristow and Rühl, 1994)

$$\frac{\partial P(\mathbf{x},\omega)}{\partial x_3} = \frac{(-i\omega)}{c(\mathbf{x})}\sqrt{1+\frac{c^2(\mathbf{x})}{\omega^2}\frac{\partial^2}{\partial x_1^2}}P(\mathbf{x},\omega)\ . \tag{1}$$

where $P(\mathbf{x},\omega)$ is the pressure wavefield, $c(\mathbf{x})$ is the medium propagation velocity. For vertically inhomogeneous media, the operator above has an exact representation in the Fourier domain (Gazdag (1978)). For laterally inhomogeneous media, a formal representation for this operator is based on the Padé expansion (Bamberger et al., 1988)

$$\sqrt{1+Z} = 1+\sum_{n=1}^{N}\frac{a_n Z}{1+b_n Z}\ , \tag{2}$$

where $Z \equiv \frac{c^2(\mathbf{x})}{\omega^2}\frac{\partial^2}{\partial x_1^2}$. The coefficients a_n and b_n are (Bamberger et al., 1988)

$$a_n = \frac{2}{2N+1}\sin^2\frac{n\pi}{2N+1} \qquad \text{and} \qquad b_n = \cos^2\frac{n\pi}{2N+1}\ . \tag{3}$$

If $Z<-1$ in equation (2), the left side is a pure imaginary number while the right side remains a real-valued quantity. In other words, the approximation breaks down. Physically, this means that representation (2) cannot properly handle evanescent modes. This causes numerical instabilities and is responsible for the unstable behavior of the FFD algorithm in the presence of high velocity variations (Biondi, 2002).

To overcome these limitation, Millinazzo et al. (1997) proposed a complex representation of the Padé expansion in equation (2). They achieve this goal by rotating the branch cut of the square root in the complex plane. Their final expression is

$$\sqrt{1+Z} \approx R_{\alpha,N}(Z) = C_0+\sum_{n=1}^{N}\frac{A_n Z}{1+B_n Z}\ , \tag{4}$$

where

$$A_n \equiv \frac{a_n e^{-i\alpha/2}}{\left[1+b_n(e^{-i\alpha}-1)\right]^2}\ , \qquad B_n \equiv \frac{b_n e^{-i\alpha}}{1+b_n(e^{-i\alpha}-1)}\ ,$$

and

$$C_0 = e^{i\alpha/2}\left[1+\sum_{n=1}^{N}\frac{a_n(e^{-i\alpha}-1)}{[1+b_n(e^{-i\alpha}-1)]}\right]\ ;,$$

with a_n and b_n as defined in equation (3). A_n and B_n are the complex Padé coefficients and α is the rotation angle of the branch cut of the square root in the complex plane.

Complex FD and FFD migration

We use the complex Padé approximation (4) to represent the one-way continuation operator. Using this approximation the downward continuation operator for finite difference migration is

$$\frac{\partial P(\mathbf{x},\omega)}{\partial x_3} = \frac{(-i\omega)}{c(\mathbf{x})}\left[C_0+\sum_{n=1}^{N}\frac{A_n\frac{c^2(\mathbf{x})}{\omega^2}\frac{\partial^2}{\partial x_1^2}}{1+B_n\frac{c^2(\mathbf{x})}{\omega^2}\frac{\partial^2}{\partial x_1^2}}\right]\ P(\mathbf{x},\omega)\ . \tag{5}$$

The FFD approximation for the downward continuation operator is deduced following the derivation proposed by Ristow and Rühl (1994). The final result is

$$p\sqrt{1+X^2} \approx \sqrt{1+p^2X^2}+C_0(p-1)+\sum_{n=1}^{N}\frac{A_n p(1-p)X^2}{1+\sigma B_n X^2}\ , \tag{6}$$

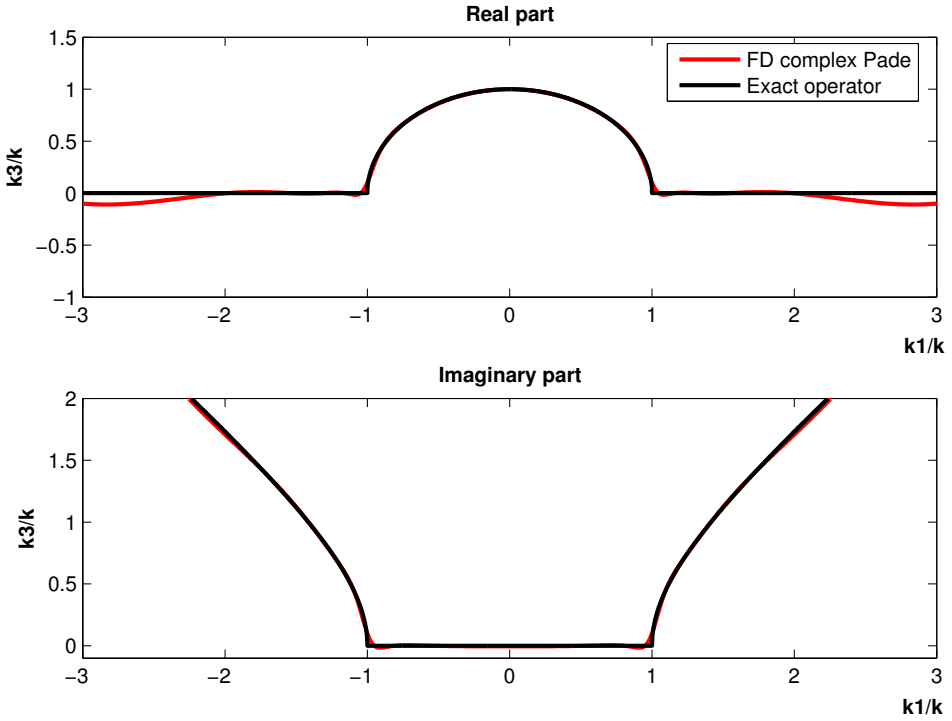

Figure 1: Complex Padé FD approximation for the dispersion relation of the one-way wave equation, computed with three terms and $\alpha = 90^o$.

where $p \equiv \frac{c_r}{c(\mathbf{x})}$ is the ratio between the actual propagation velocity, $c(\mathbf{x})$, and the propagation velocity in an homogeneous background medium, c_r. Moreover, $X^2 \equiv \left(\frac{c}{\omega}\right)^2 \frac{\partial^2}{\partial x_1^2}$ and $\sigma = 1 + p + p^2$.

Based on numerical experiments comparing the exact operator and the FFD approximation, we propose to use $\sigma = 1 + p^3$ for wide-angle approximations, instead of $\sigma = 1 + p + p^2$.

NUMERICAL EVALUATIONS

To better understand the involved approximations, we numerically evaluate the dispersion relations of the wide-angle FD and FFD approximations and compare them with the exact dispersion relation. We complement our numerical evaluation computing the impulse response of our approximations in a homogeneous medium. Finally, we compare the impulse response of the proposed wide-angle complex FD and FFD algorithms with the unconditionally FFD algorithm proposed by Biondi (2002).

Dispersion relation

ure 1 shows the comparison of the exact dispersion relation with its FD approximation 2. The FD approximation was calculated using the first three terms of the series with a rotation angle $\alpha = 90^o$. The complex Padé approximation fits the real and imaginary part of the dispersion relation almost perfectly. In other words, it correctly represents the evanescent modes.

ure 2 shows the comparison of three FFD approximations for the one-way wave equation dispersion relation, with the exact dispersion curve: FFD using real coefficients, complex FFD with $\sigma = 1 + p + p^2$ and complex FFD using $\sigma = 1 + p^3$. The FFD approximations were determined using $p = 0.5$ and three terms in the Padé expansion. For the complex Padé approximation, we used a rotation angle of $\alpha = 45^o$.

The real part of the FFD operator using the real-valued Padé expansion (2) is clearly affected by spurious oscillations in the evanescent region. The complex FFD attenuates evanescent modes and, moreover,

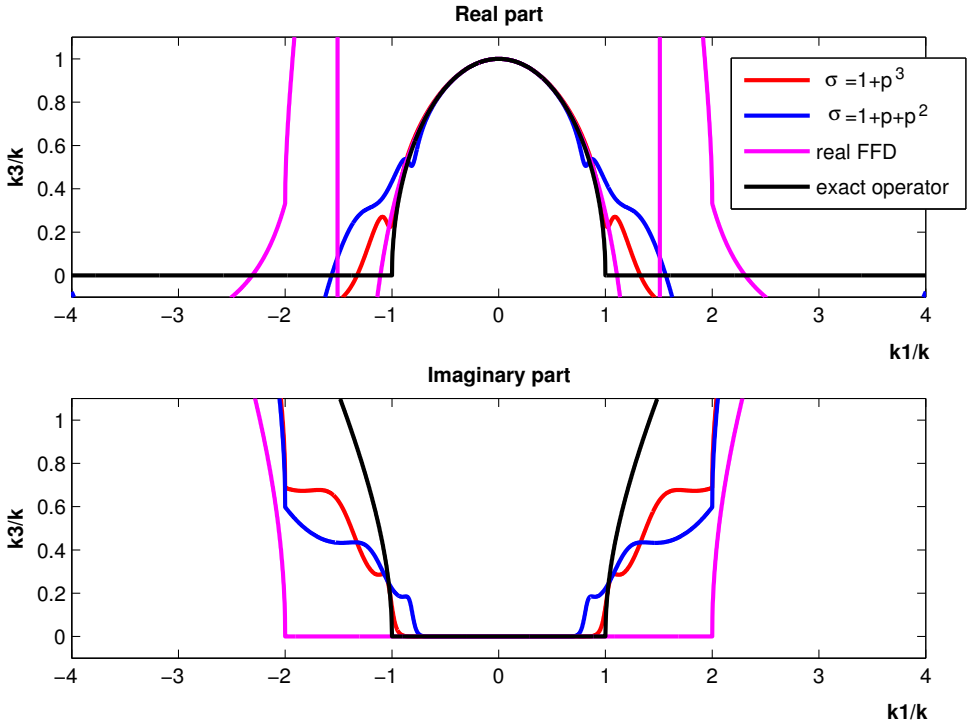

Figure 2: FFD approximations for the one-way wave equation dispersion relation. Notice the spurious oscillations of the real-valued Padé expansion for the propagating modes. The FFD not only attenuates evanescent modes, but also propagating modes which are not well approximated.

the attenuation starts where the approximation of propagating modes begins to lose its accuracy. When replacing the definition of σ by $\sigma = 1 + p^3$, the FFD approximation remains close to the exact dispersion relation for higher propagation angles. We therefore refer to this choice of σ as the wide-angle approximation.

Impulse response

ure 3 shows the impulse responses of the wide-angle complex FD and FFD approximations for a homogeneous medium. We used a Ricker pulse with peak frequency of 25 Hz. We computed the FD impulse response using three terms in the Padé expansion and $\alpha = 90^o$. The reference velocity was the true medium velocity. For the FFD impulse response, we also used three terms in the Padé expansion, with $p = 0.5$ and $\alpha = 45^o$. These parameters were selected based on the numerical experiments for the approximations of the dispersion relation. The reference velocity for FFD was half the true medium velocity. Both impulse responses have energy up to high propagation angles. Note that the wide-angle FFD approximation recovers the impulse response quite well, in spite of the wrong reference velocity. Note, however, that some high-frequency content is lost and the wavelet is no longer perfectly symmetric. These effects become weaker the closer the reference velocity is to the true medium velocity.

To evaluate the performance of the wide-angle complex FD and FFD approximations in an inhomogeneous medium, we compare their results in the Marmousi velocity model without smoothing. As a reference, we also compare the results to those of standard real-valued FFD and of the unconditionally stable FFD algorithm proposed by Biondi (2002) in the same model. Since the latter algorithm incorporates a FFD migration plus interpolation, we refer to it as FFDPI migration. As before, the source pulse is a Ricker with peak frequency 25 Hz. The impulse responses were computed with the same parameters as used in the homogeneous medium.

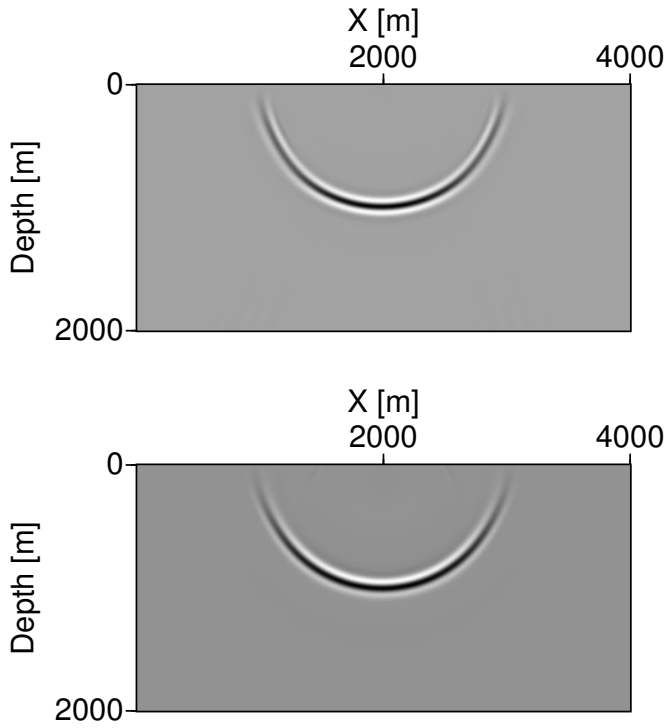

Figure 3: Impulse responses in a homogeneous medium for FD (top) and FFD (center) migration. using wide-angle complex Padé approximations, compared to the real-valued FFD approximation (bottom).

ures 4, 5, 6, and 7 show the impulse responses of the complex wide-angle FD and FFD approximations, as well as real-valued FFD and FFDPI, respectively. All responses are similar if we only consider the most energetic events. The results of wide-angle complex FFD are closer to the FFDPI than those of the wide-angle complex FD. Note that wide-angle complex FFD covers higher angles than FFDPI. Here, frequency content and wavelet shape of the wide-angle complex FFD are practically identical to that of FFDPI, because the reference velocities are chosen based on the true velocity model. The real-valued FFD approximation clearly provides the worst results. It contains non-negligible non-causal energy and even some upgoing events.

There are a few events that appear differently in the complex FFD and FFDPI impulse responses. The most obvious difference is a dipping event to the right of the main wavefront, which appears only in FFDPI. Since it leaks in front of the main wavefront, it seems to be a spurious, non-causal event. Secondly, the event on the top left of the impulse response appears with a slightly different dip. Here, the wide-angle approximation of the complex FFD seems to better preserve the true, nearly vertical dip. Finally, there is a weak horizontal event inside the main wavefront, slightly to the right, which appears stronger in the FFDPI than in the complex FFD. Here, FFDPI seems to better preserve the event.

In conclusion, the approximations obtained from complex FFD and FFDPI are of comparable quality, each one preserving slightly different features of the impulse response. The real-valued FFD and complex FD approximations are of inferior quality.

MIGRATION RESULTS

We have implemented the wide-angle complex FD and FFD approximations to perform pre-stack depth migration in 2D. We have also implemented the FFDPI migration of Biondi (2002) for comparison. The imaging condition is the crosscorrelation of the downward continued upgoing wavefield and downgoing wavefield from source at zero time lag. Other imaging conditions that correct for the illumination are being tested (Schleicher et al., 2006). The source wavefield is computed using a Ricker wavelet with 25 Hz peak

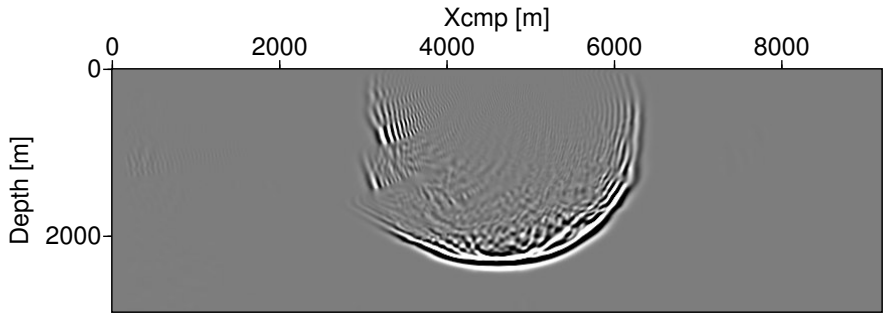

Figure 4: Impulse response of wide-angle complex FD in the Marmousi velocity model.

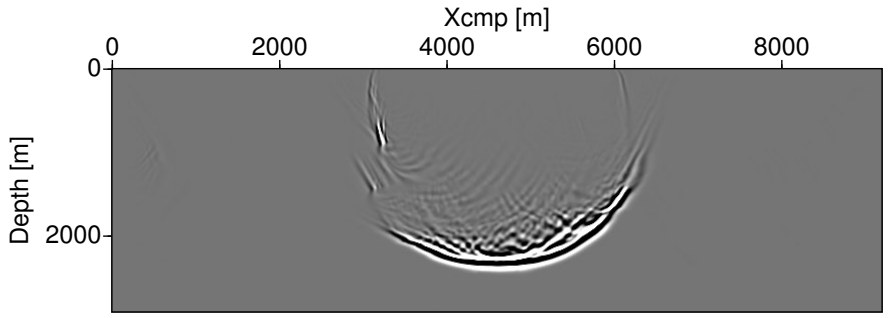

Figure 5: Impulse response of wide-angle complex FFD in the Marmousi velocity model.

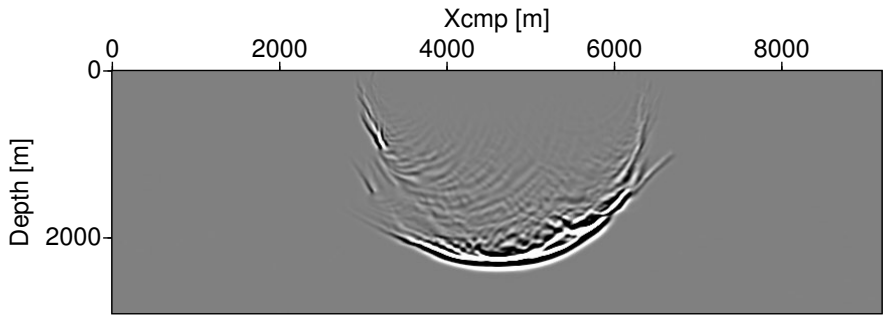

Figure 6: Impulse response of FFDPI in the Marmousi velocity model.

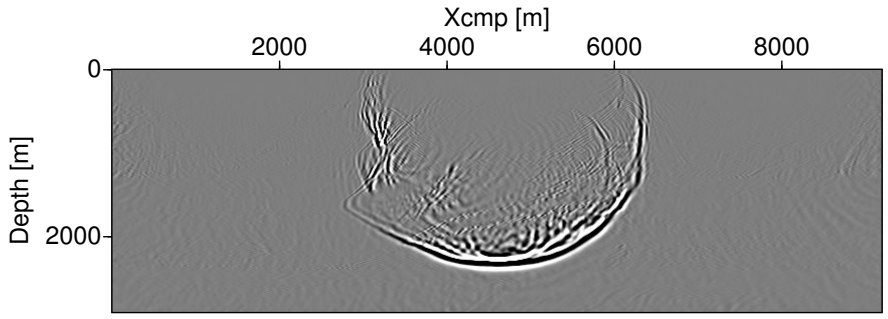

Figure 7: Impulse response of real-valued FFD in the Marmousi velocity model.

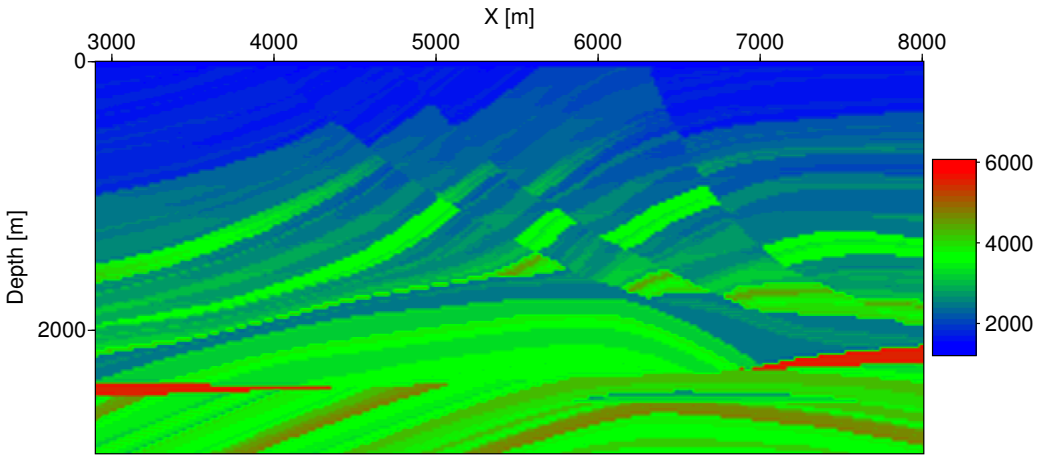

Figure 8: Marmousi velocity model.

frequency. The complex FD and FFD approximations are computed with the same parameters as previously selected.

As our first test, we migrated the Marmousi dataset using the true Marmousi velocity model (Versteeg, 1994), without any smoothing (see ure 8). ure 9 shows the result of wide angle complex FD migration. The depth extrapolation step size for both complex FD and FFD is 6 m. ure 10 shows the result of the wide angle complex FFD migration. ure 11 shows the FFDPI results. The requirement of velocity interpolation makes FFDPI computationally more expensive. To reduce the cpu time, we used a depth extrapolation step of 12 m for FFDPI migration. Still the FFDPI migration takes twice as much cpu time as the complex FFD algorithm. The images are overall very similar. The complex FD image is a little more blurred at the target reservoir region and fails to resolve the faults as well as complex FFD and FFDPI. Though there are some slight differences between the images of the latter two methods, its impossible to tell which of the two images is better. This is in agreement with our findings when studying the impulse responses. For comparison, ure 12 presents the result of FFD migration using the seismic un*x FFD algorithm Cohen and Stockwell (2006). The depth interval was also 6 m. Though it seems to preserve higher frequencies, the image is overall of inferior quality. Moreover, the algorithm suffers from instabilities and numerical dispersion and strongly distorts the source wavelet.

For another comparison between the complex FFD and the FFDPI algorithms, we also applied the proposed algorithms to synthetic data from the SEG/EAGE salt model (Aminzadeh et al. (1995)). We used a 2D dataset computed using the 2D section of the 3D model shown in ure 13. ure 14 and ure 15 show the complex FD and FFD migration results, respectively. In this model, which has a simpler structure than the Marmousi model, both techniques based on the complex Padé expansion provide results of comparable quality. Because of the high quality of the images from complex FD and FFD migration and the high computational cost of FFDPI, we refrained from carrying out the latter for this larger model.

CONCLUSIONS

We applied the complex Padé approximation (Millinazzo et al., 1997) to derive wide-angle complex finite-difference (FD) and Fourier finite-difference (FFD) migrations. The complex Padé approximation, which is based on a rotation of the branch cut for the square root in the one-way wave propagator, attenuates evanescent waves, thus solving the problems with numerical instabilities of real-valued FD and FFD migration algorithms.

Based on numerical experiments with impulse responses and full migrated images, we have found that three terms in the Padé expansion are sufficient for wide-angle approximations of acceptable quality. These numerical experiments have also indicated that the most adequate rotation angle of the branch cut is $\alpha = 90^o$ for FD and $\alpha = 45^o$ for FFD migration, though more exhaustive tests are required using different

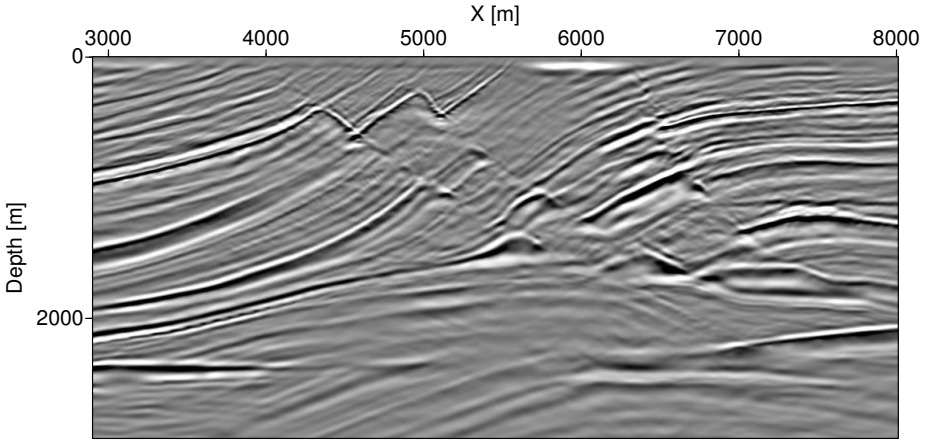

Figure 9: Pre-SDM of Marmousi dataset using wide angle complex FD.

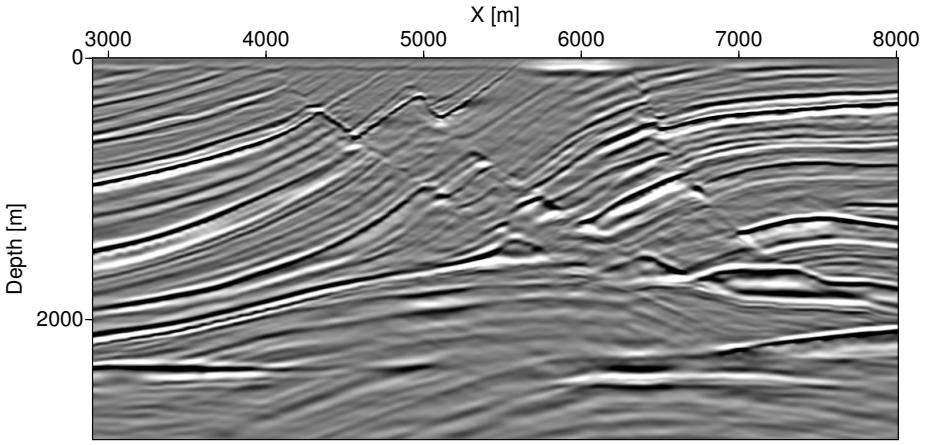

Figure 10: Pre-SDM of Marmousi dataset using wide angle complex FFD. Notice the stability of the complex FFD approximation.

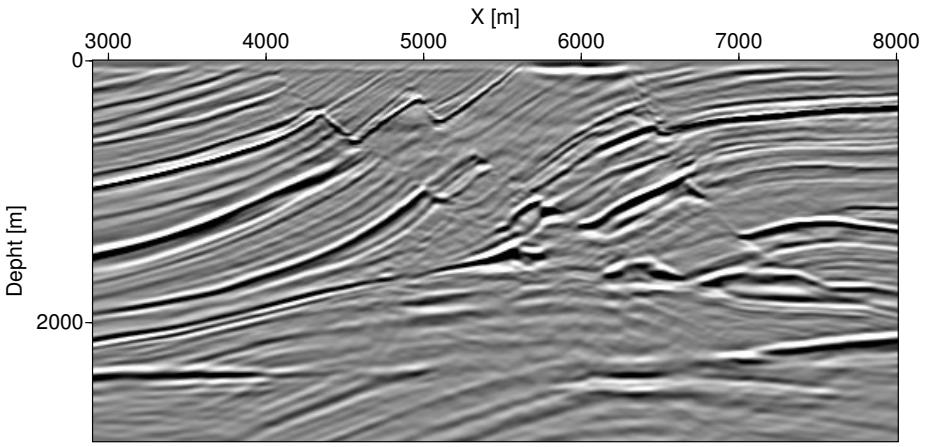

Figure 11: Pre-SDM of Marmousi dataset using wide angle FFDPI.

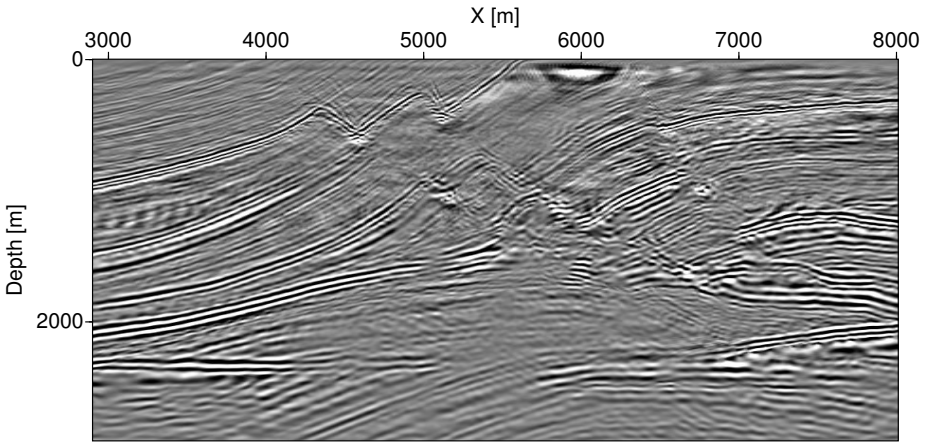

Figure 12: Pre-SDM of Marmousi data set using the SU algorithm based on the real-valued Padé expansion. The image suffers from numerical dispersion and instabilities.

velocity models to validate this prescription. Moreover, our numerical experiments have demonstrated that choosing $\sigma = 1 + p^3$ instead of $\sigma = 1 + p + p^2$ in the complex Padé expansion [equation (6)] improves the wide-angle approximations.

Results of the application of the proposed algorithms to synthetic data from the Marmousi and the SEG/EAGE salt models indicate that the wide-angle complex FD and FFD migrations are stable algorithms even in complicated velocity models, where real-valued FFD algorithms fail to provide stable results. For the Marmousi model, the migrated images from complex FD and FFD migrations were very similar to the images obtained with the results of the unconditionally stable Fourier finite-difference plus interpolation (FFDPI) migration of Biondi (2002). The proposed algorithms are computationally less expensive. The complex FFD algorithm with half the step size used in the FFDPI algorithm was twice as fast. The complex FD migration is about another 30% faster.

ACKNOWLEDGMENTS

This research has been supported by FINEP, CNPq, CENPES/PETROBRAS and the sponsors of the Wave Inversion Technology (WIT) Consortium.

REFERENCES

Aminzadeh, F., Burkhard, N., Nicoletis, L., and Rocca, F. (1995). 3-d modeling project 3rd report. *The Leading Edge*, 14:125–128.

Bamberger, A., Engquist, L. H., and Joly, P. (1988). Higher order paraxial wave equation approximations in heterogeneous media. *J. Appl. Math.*, 48:129–154.

Biondi, B. (2002). Stable wide-angle fourier finite-difference downward extrapolation of 3-d wavefields. *Geophysics*, 67(3):872–882.

Cohen, J. K. and Stockwell, J. J. W. (2006). *CWP/SU: Seismic Un*x Release 39: a free package for seismic research and processing*. Center for Wave Phenomena,Colorado School of Mines.

Gazdag, J. (1978). Wave equation migration with the phase-shift method. *Geophysics*, 73:1342–1351.

Millinazzo, F. A., Zala, C. A., and Brooke, G. H. (1997). Square-root approximations for parabolic equation algorithms. *J. Acoust. Soc. Am.*, 101(2):760–766.

Ristow, D. and Rühl, T. (1994). Fourier finite-difference migration. *Geophysics*, 59(12):1882–1893.

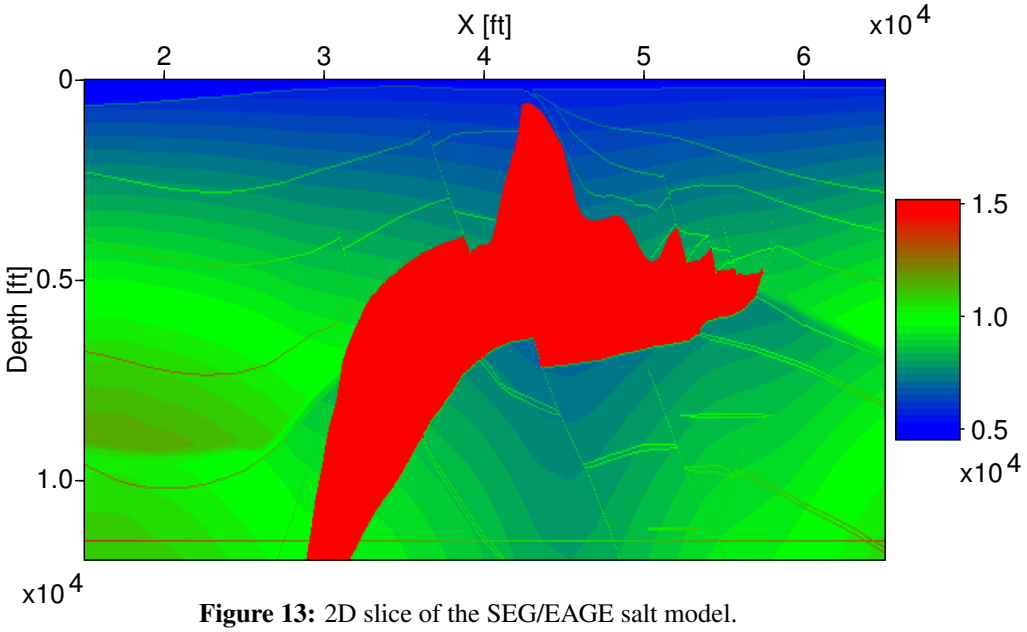

Figure 13: 2D slice of the SEG/EAGE salt model.

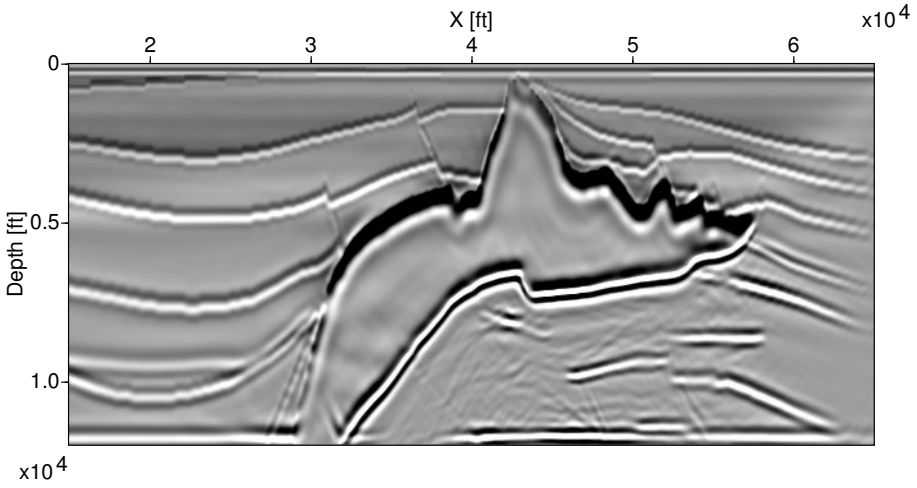

Figure 14: Pre-SDM from SEG/EAGE 2D data set using complex FD.

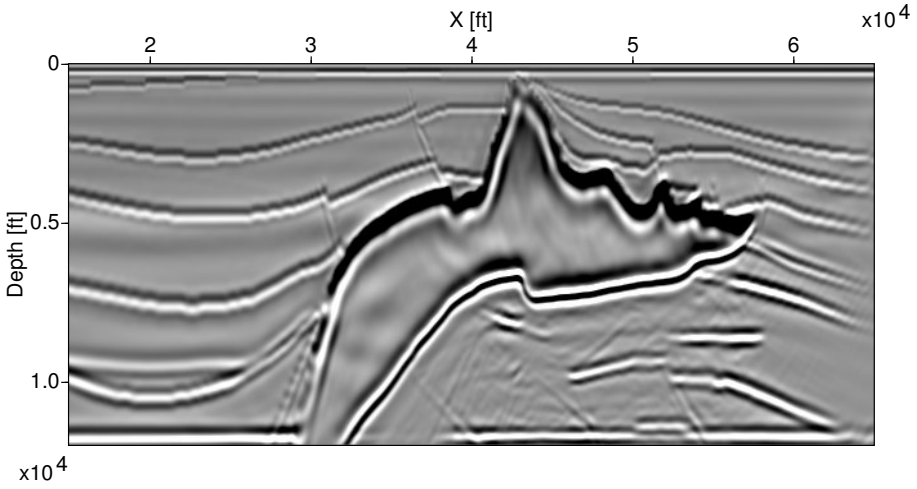

Figure 15: Pre-SDM from SEG/EAGE 2D data set using complex FFD.

Schleicher, J., Costa, J. C., and Novais, A. (2006). A comparison of imaging conditions for wave-equation shot-profile migration. *Annual WIT Report*, 10:159–171 This issue.

Versteeg, R. (1994). The marmousi experience: velocity model determination on a synthetic complex data set. *The Leading Edge*, 13:927–936.

Zhang, L., Rector, J. W., and Hoversten, G. M. (2003). Split-step complex padé migration. *Journal of Seismic Exploration*, 12:229–236.

Zhang, L., Rector, J. W., Hoversten, G. M., and Fomel, S. (2004). Split-step complex padé-fourier depth migration. *SEG Int'l Exposition and 74th Annual Meeting*.